LES of Turbulent Mixing of Non Reacting Flow in a Gas Generator

Changjin Lee
School of Aerospace Engineering, Konkuk University, Seoul, Korea, 143-701

cjlee@konkuk.ac.kr

Keywords: Gas generator, LES, turbulent mixing, turbulence ring

Abstract

LES analysis was conducted with in-house CFD code to investigate the turbulence evolution and interaction due to turbulence ring and splash plate in the gas generator. Though chemical reaction was not accounted for, the results can be useful in determining the turbulence characteristics generated by ring and plate. The calculation results show that the installation of turbulence ring can introduce additional turbulences and improve turbulent mixing in the downstream flow. However, the addition of splash plate in the downstream of TR brings totally different shape of perturbation energy and enstrophy distribution for turbulent mixing. This enhancement can be done by the formation of the intensively strong vorticity production and mixing behind the plate. Pressure drop was found to be a reasonable level of about 1% or less of initial pressure in all calculation cases. Also, calculation results revealed that the variation of TR shape and intrusion length did not change the characteristics of turbulent mixing in the chamber. Even though the effect of installation location of splash plate on the turbulent mixing is not investigated yet, calculation results conclude the addition of splash plate leads to the increase in turbulent mixing with an acceptable pressure drop.

1. Introduction

The rocket propellants are usually fed into the thrust chamber by either gas-pressurized feed system or turbopump feed system. Even though pressurized feeding system has advantages of simplicity in operation, the turbopump feed system is suitable for high thrust, long duration engines. In turbopump feed system, the major portion of the pressure required to feed propellants is supplied by pumps. Therefore, the turbopump system can be essentially applied to large liquid rocket engine (LRE) system with the improved performance[1,2,3]. Generally, the delivered temperature from gas generator should be maintained about 1000K or less to avoid any excessive thermal stress on turbine blades since no cooling system could be installed in turbopump system. Thus, the operational condition of gas generator is generally either fuel-rich or oxidizer rich combustion[2] to maintain the combustion temperature within the allowable range. So, the temperature uniformity in the chamber and the vaporization of fuel droplet become critical issues in designing the combustion chamber. Turbulence ring (TR) can be used to achieve mixing enhancement prior to turbine entrance.

Figure 1 shows a schematic of vaporization curve of fuel and liquid oxidizer in fuel rich mixture. Since the oxidizer vaporizes more quickly, most of stoichiometric chemical reaction takes place in the very narrow region near the injector plate. The decomposition of excessive fuel in the gaseous oxygen environment is followed in the rest of combustion chamber. Also, turbulent mixing of hot burnt gas and excessive vaporized fuel causes the endothermic fuel decomposition leading to a gradual temperature decrease in the downstream of combustor. However, the stoichiometric combustion near injector plate produces hot temperature streaks causing the temperature stratification. Thus turbulence ring can be used to provide an additional mixing condition in order to eliminate hot streak formation which causes the thermal stress on the turbine blade. The generation of vortex can enhance the turbulent mixing of combustion gas and vaporized excessive fuel and lead to the spatially uniform temperature profile prior to turbine inlet. In this respect, the location and configuration of turbulence ring can be an issue in the preliminary design stage even though many liquid rocket engines already adopted various types of TR in the gas generator. Also, it should be noted that the design criteria on the configuration of TR is rarely available in the public domain.

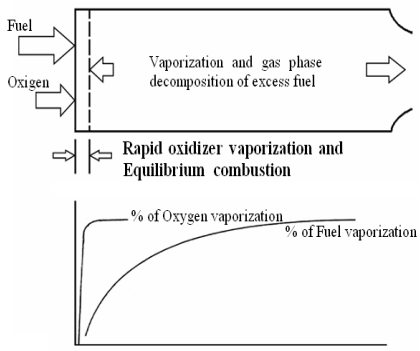

Fig 1. Schematic of fuel and oxidizer evaporation curve in gas generator

A few experimental tests and numerical calculations had been done with various TR configurations to investigate the role of TR on the improvement of spatial temperature profile. [12-15] And results could prove that the use of turbulence ring can dramatically improve the temperature uniformity at the chamber

exit. Lawver et al. [14] conducted a series of experiments for the design and the integration of gas generator system by adopting TR. The primary purpose of the study was focused on the development of performance evaluation of a gas generator. And they measured temperature and pressure profiles in the combustion chamber and found the installation of TR could suppress the pressure oscillations and hot spots effectively. However, the design guideline of TR was not revealed in the literature. Figure 2 shows the effect of TR installation on the suppression of temperature oscillations measured by Lee et al. [15] Kim had performed RANS calculations for several test cases to investigate the combustion efficiency and pressure drop to find the optimal the combination of TR and splash plate. [17] His calculation revealed the addition of splash plate could improve temperature uniformity if the location was properly selected. However, RANS calculation only provides the average value of turbulent mixing in the chamber, and the vortical structures cannot be captured in the calculation. Thus, RANS results provide only qualitative descriptions of turbulent mixing. Furthermore, calculation results were not verified by any other experimental data.

In this regard, LES is appropriate to understand instantaneous mixing mechanisms associated with vortical structures generated by TR and splash plate. Also, Fureby et al. [1] had studied the mixing enhancement and combustion characteristics in afterburner by using flame wrinkling LES combustion model. His calculation results showed LES is a promising approach to broaden the understanding of mixing mechanism of turbulent flow.

As aforementioned, it is very difficult to simulate the turbulent combustion in a gas generator including every physical phenomenon such as non-equilibrium chemistry, fuel decomposition, turbulent combustion, and mixing. However, the heat generation occurs only within the limited region near injection plate and non-reacting turbulent mixing dominates in the rest of gas generator. Thus, it is plausible to assume that the analysis of non-reactive turbulent flow can yield the design guideline of how to improve mixing mechanism in the chamber if various TR configurations and splash plate could be used.

The present study mainly concerns the analysis of non-reacting turbulent flow mixing in gas generator. Various TR configurations and splash plates were used to investigate the vortical flow structures and mixing characteristics in the downstream. To this end, a LES calculation code was developed and verified its validity. Also, the role of splash plate in generating turbulences was quantitatively investigated by comparing with the analysis results implemented with TR. The comparison of calculation results of turbulent energy and enstrophy could provide the basic understanding on the evolution of vortical structures associated with mixing mechanism and the guide line of how much mixing improvement can be achieved by the use of mixing enhancement devices in the primary design stage.

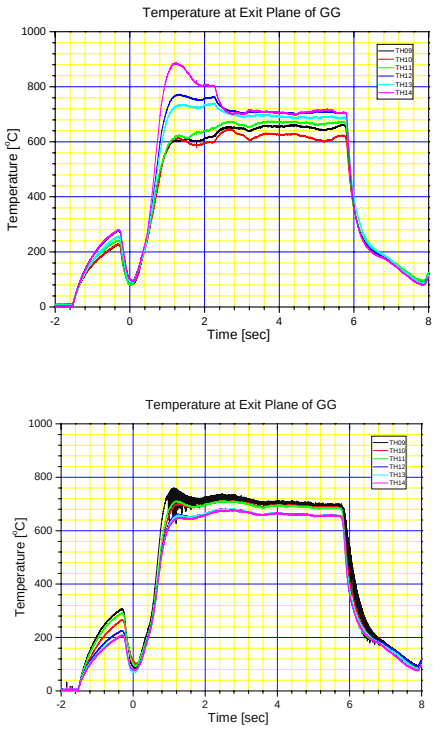

Fig 2. Comparison of temperature profiles measured with and without TR installation

2. LES Code

The development of LES code for non-reacting turbulent flow in the gas generator was initiated by solving a set of filtered governing equations. It is worth noting that LES code was designed to apply to both compressible and incompressible flow conditions with generalized coordinate system. Time-derivative preconditioning method is one of techniques used to reduce convergence problems frequently observed in low Mach number flows [2,3]. The preconditioned 3-D compressible Navier-Stokes equations are:

$$\Gamma\frac{\partial Q}{\partial t} + \frac{W}{t} + \frac{\partial(F_j - F_{vj})}{x_j} = 0 \qquad (1)$$

where F_j and F_{vj} are inviscid and viscous fluxes in each direction, respectively

$$Q = \begin{Bmatrix} p \\ u_i \\ T \end{Bmatrix}, \quad W = \begin{Bmatrix} \rho \\ \rho u_i \\ \rho E \end{Bmatrix}, \quad F_j = \begin{Bmatrix} \rho u_j \\ \rho u_i u_j + p\delta_{ij} \\ \rho u_j H \end{Bmatrix}, \qquad (2)$$

$$F_{vj} = \begin{Bmatrix} 0 \\ \tau_{ij} + \tau^*_{ij} \\ (\tau_{ij} + \tau^*_{ij})u_i - q_j + (\mu + \sigma_k \mu_t)\frac{\partial k}{\partial x_j} \end{Bmatrix}$$

The quantity τ_{ij} and τ^*_{ij} denote the laminar and turbulent stresses, respectively, and q_j represents the total heat flux in each direction. These quantities can be defined as:

$$t_{ij} = 2\mu_t\left(S_{ij} - \frac{1}{3}S_{kk}\delta_{ij}\right),$$
$$t^*_{ij} = 2\mu_t\left(S_{ij} - \frac{1}{3}S_{kk}\delta_{ij}\right) - \frac{2}{3}\rho k\delta_{ij} \quad (3)$$
$$q_j = -\frac{\gamma R}{(\gamma-1)}\left(\frac{\mu}{\mathrm{Pr}_l} + \frac{\mu_t}{\mathrm{Pr}_t}\right)\frac{\partial T}{\partial x_j}$$

Here the eddy viscosity, μ_t, is defined based on the used turbulence model. The term S_{ij} is defined as:

$$S_{ij} = \frac{1}{2}\left(\frac{\partial u_i}{\partial x_j} + \frac{\partial u_j}{\partial x_i}\right) \quad (4)$$

The preconditioning matrix Γ is a conventional one suggested by Choi and Merkle [4] and extended by Weiss et al. [2]:

$$\Gamma = \begin{bmatrix} \Theta + 1/(RT) & 0 & 0 & -\rho/T \\ u[\Theta + 1/(RT)] & \rho & 0 & -\rho u/T \\ v[\Theta + 1/(RT)] & 0 & \rho & -\rho v/T \\ H[\Theta + 1/(RT)] - 1 & \rho u & \rho v & \rho\frac{\partial \rho}{\partial p} - \rho H/T \end{bmatrix} \quad (5)$$

where the parameter Θ is defined as:

$$\Theta = \frac{1}{U_r^2} - \frac{1}{a^2} \quad (6)$$

The reference velocity has been chosen as shown in equation (7) to avoid any unstable solution behaviors at near-stagnation regions and to easily recover the original equations at supersonic flow regions. In the present study, an unsteady limitation [6, 7] to an optimized steady preconditioning [3] was also applied:

$$U_r = \min\left[\max\left(|U|, KU_{cut}, \frac{\mu}{\rho\Delta d}, \sqrt{\frac{|p'|}{\rho}}, \frac{L}{\rho\Delta t}\right)\right] \quad (7)$$

Here $U_{cut} = min\ (U_\infty, a_\infty)$. And $p' = (p_l + p_r)/2$ is the definition and p_l, p_r are gauge pressures of left and right at the adjacent cell, respectively. The unsteady preconditioning matrix varies with physical time step. As the time step increases, it approaches to steady state. This unsteady preconditioning scales the artificial dissipation in the flux function as well as improves pseudo-time convergence efficiency regardless of the choice of physical time step [8].

Developed LES code can treat parallelized multi-block grid system to increase the calculation efficiency implemented with MPI technique for 55 CPU. Also, a low diffusive centralized scheme is used to reduce error accumulation by adopting the high order skew-symmetric central fluxes. This method can alleviate odd-even decoupling error frequently observed in collocated grid system. Dual-time stepping with a DADI method is used to advance the solution in time. This allows one not only to use a large time increment, but also to maintain temporal accuracy. The dual-time stepping also can eliminate factorization and linearization errors introduced by the iteration of solutions along a pseudo-time. Details of the numerical methods and techniques implemented in the code can be found in the reference [3].

Dynamic Smagorinsky Model

The well-known Smagorinsky model based on Boussinesq's approach was used in the developed LES code. In the analogy to viscous stresses in laminar flow, the turbulent stresses are assumed proportional to the mean velocity gradients, or more general to the large-scale strain rate tensor S_{ij}:

$$t^a_{ij} = t_{ij} - \delta_{ij}\frac{t_{kk}}{3} = -2\mu_t\left(S_{ij} - \frac{1}{3}S_{kk}\delta_{ij}\right) \quad (8)$$

where τ^a_{ij} is the anisotropic traceless part of the subgrid scale Reynolds stresses. The trace of the stress tensor needs to be modeled or estimated. The eddy viscosity itself is a function of the strain rate tensor S_{ij} and the sub grid length l as:

$$\mu_t = \rho l^2|\bar{S}|, \quad |\bar{S}| = \sqrt{2\bar{S}_{ij}\bar{S}_{ij}} \quad (9)$$

The subgrid length l is assumed to be proportional to the filter width Δ:

$$l = C_s\bar{\Delta} = C_s(\Delta x\Delta y\Delta z)^{1/3} = C_s(1/J)^{1/3} \quad (10)$$

where C_s is the Smagorinsky constant and $1/J$ is the volume of the cell.

Code Verification

The verification test was done with the well known cylindrical channel flow by comparing the accuracy of calculation results of the channel flow. Figure 3 shows the comparison of calculation results with log-law and stochastic of u and v rms. As seen in figure, more accurate results can be obtained with 4th-order FV skew-symmetric central fluxes than with 2nd-order scheme. Nevertheless, two schemes can yield the same accuracy if (newly developed) 3rd- and 5th-order pressure diffusion terms were used for the elimination of odd-even decoupling in collocated grid. The calculation was done at Re=23,000, the same Reynolds number as in the experiments [15]. Grid system consists of 64x96x128 points, which did not produce any irrelevant numerical errors depending on the number of grid points. The averaged value was compared after the flow fully developed into turbulent flow.

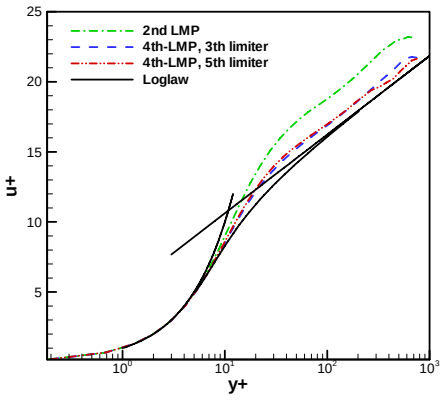

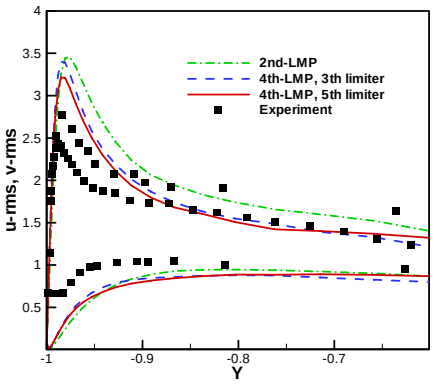

Fig 3. Comparison of mean velocity and turbulent intensity distribution by developed code with well known log-law behavior and experimental results

3. Numerical Calculations

Table 1 summarizes configurations of turbulence ring used in the numerical calculation. The baseline gas generator has the dimension of 52x300 (mm) and the case 1 to 3 are selected to have the same intrusion length in order to investigate the effect of the cross sectional shape on the mixing characteristics. Case 4 was designed to investigate how much the mixing can be improved with an extended length and the addition of splash plate to the downstream of TR was studied in case 5. Kim reported that the properly selected location of splash plate could dramatically increase the mixing efficiency in the RANS calculation. However, their results showed the temperature profiles and pressure drops of various cases along the centerline. But the comparison of the extent of mixing in the turbulent flow was not made. Thus, the present study will focus on the mixing enhancement by using the evolution of vortical structures generated by TR and splash plate, respectively. Also, the comparison of vortical structures of each case can show the intrinsic features of vorticity generation and mixing mechanism in turbulent flow. In all calculations, Reynolds number is fixed as 23,000, which is the same number used in the combustion tests in [15] and grid points was set with more than about 3 million points of 225x121x129. Moreover, the LES calculation was performed by multi-block parallel algorithm based on MPI (Message passing interface) technique to effectively reduce the calculation resources. And the total number of 55 CPU was used for the calculation of combustor equipped with turbulence ring.

Table 1. Summary of various configurations of TR

	case 1	case 2	case 3	case 4	case 5
Shape					case 1 + splash plate
length(mm)	6.8	6.8	6.8	8.6	

In the computation, two additional ducts were attached to the inlet and exit plane. Theoretically, the combustion in a gas generator is a constant pressure process. However, heat addition, so called Rayleigh flow, and viscous dissipation in turbulent flow causes pressure drops in the combustion chamber. In the preliminary design stage, the estimation of pressure drop in the chamber is one of the important things to determine the combustion performance. And the guide line of pressure drop in a gas generator is less than 5% of initial pressure. Figure 4 shows the computational domain and temporal ducts with grid system. Temporal duct at inlet plane can be used to make a fully developed turbulent flow by using the periodic boundary conditions prior to the main combustor. However, the use of boundary condition leads to continuous pressure drops during the iteration process in the temporal duct. To eliminate the pressure drop in the temporal duct, a proper treatment of pressure loss is required prior to main chamber. Also, the exit plane in computational domain may create unnecessary pressure behavior bouncing back into main chamber during the numerical calculation. The bounced pressure wave can cause the unphysical interaction with pressure field in the combustor and lead to distorted pressure losses. Thus, the temporal duct attached to exit plane of main chamber should provide an enough axial space to delay the bouncing pressure wave from the exit plane until the correct pressure filed can be calculated. Thus, LES calculation can yield the correct estimation of pressure drop in the chamber by the use of two temporal ducts.

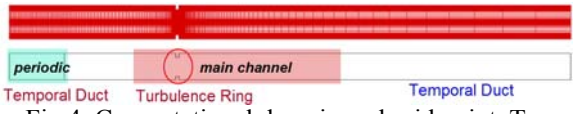

Fig 4. Computational domain and grid point. Two temporal ducts are attached artificially

4. Results and Discussion

Figure 5 shows the summary of instantaneous axial velocity and vorticity profile of all calculation cases on the center section of cylinder. Red color represents flow velocity in streamwise direction while blue color is negative velocity. Similar flow patterns of axial velocity profiles are observed in case 1 to 3, even though three cases used different TR shapes respectively. A strong core jet flow is formed in the downstream because TR blocks flow passage. Also, TR produces negative velocity regions along the wall surface, which interact with core jet and generate additional turbulent kinetic energy to the flow. Case 4 shows the effect of elongation of intrusion length on the instantaneous axial velocity and vorticity profile. Even though the strength of core jet becomes stronger and TR produces more negative velocity region behind TR, the basic flow characteristics is not changed in case 4 when compared to previous cases of 1 to 3. Thus, it can be summarized that the modification of TR shape and/or intrusion length can not alter flow pattern and turbulent mixing. And turbulent mixing is expected to occur near the wall

surface by the interaction of core jet and negative wall shear flow. However, the addition of splash plate to downstream of TR generates a totally different turbulent flow pattern behind the plate as seen in case 5. A strong annular jet forms around the plate due to blocked flow passage and a big recirculation region is developed behind the plate. The mutual interaction of annular jet and recirculation flow can be a substantial source of turbulent mixing in the downstream flow.

The evolution of vortical flow structures are also seen in figure 5 for all calculation cases. Red spots in figures describe the region where vorticity is actively strong. Vorticity is closely related with turbulent mixing in the flow. Thus, the mixing can be enhanced in the region with red color in the flow. Similarly seen in the axial velocity profile, case 1 to 3 show the vortices productions are confined near wall surface in the downstream of TR. This implies most of turbulent mixing happens in the downstream flow behind TR by the interaction of core jet and wall shear flow, and the core flow was not affected by turbulent mixing. The elongation of TR length did not change the basic mechanism of turbulent mixing even though a little stronger vorticity are generated. However, the overall pattern of axial velocity and vorticity generation in case 5 totally differs from the previous cases. Splash plate acts as a source of strong vorticity generation in the region behind the plate due to the interaction between strong axial velocity stream along the wall surface and relatively stagnated flow near central region. Most of vortical structures in case 5 are found behind the plate. And the vorticity generation is enhanced by the addition of splash plate within a very short distance.

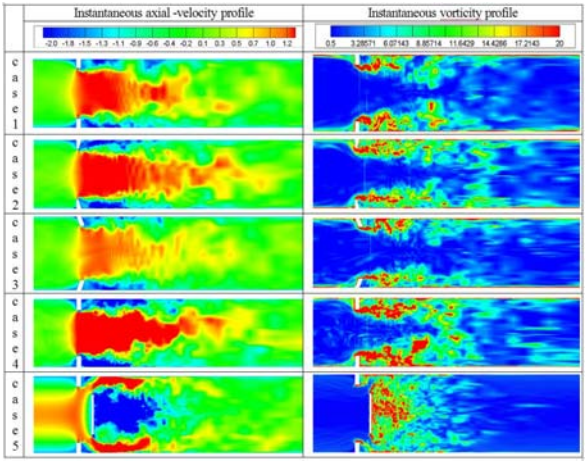

Fig 5. Instantaneous contour of axial velocity and vorticity on the center plane

Figure 6 compares the evolution of vortical structures at several axial locations in case 3 and 5. The comparison is made to investigate the basic difference of turbulent mixing mechanisms between the case with TR and the case with TR plus splash plate

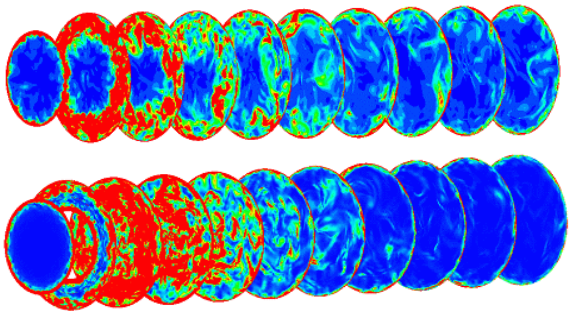

Fig 6. Comparison of vortical structure evolution in case 3 and 5

The generation of vortices in case 3 is confined in the region, where is very near the wall surface, behind TR. And the dissipative mechanism gradually weakens vorticity strength in the downstream. However, vortical structures are still observed in the core region survived up to combustor exit. The addition of splash plate shows the different evolution of vortical structures. As seen in figure 6, a certain section in case 5 is nearly filled with generated vorticity behind the plate, which diminishes quite quickly leaving no traces of vortical structures at the exit. This represents that the addition of splash plate can agitate the flow more thoroughly than TR can. It improves turbulent mixing within a very short distance. And it can be summarized that the downstream flow in case 5 becomes more uniform than that in case 3 since no fluctuations are remained.

Figure 7 can provide more detailed information on the inception of vortical structures due to TR and splash plate in terms of streamwise vorticity. This is the comparison of longitudinal vortices component 12 in case 3 and 5, which describes how vortical structures can be generated in the downstream flow.

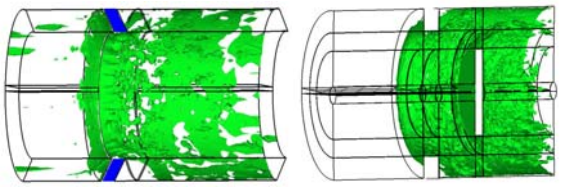

Fig 7. Iso-surface of longitudinal vorticity component ω_{12} =20 in case 3 and 5

The inception of vortical structures is clearly observed at the edge of TR in case 3. Blue color is the sectional cut of turbulence ring. As flow passes over TR, roll-up patterns of vorticity are formed at the edge and followed by the series of vortex breakup in the downstream. This can be a source of vortical structures generated by TR. Thus, the generation of vortices occurs only due to the formation of roll-up vortex, and this fact can explain why the modification of TR shapes (case 1 and 2) did not bring intrinsic changes in vorticity patterns. However, the flow patterns in case 5 shows shedding vorticity formed around the plate and a lot of small scaled vortices are observed behind the plate. This is strongly related with the turbulent mixing enhancement in case 5.

The primary concern of the current calculation is the quantitative measurement of turbulent mixing enhancement to investigate the influence of various TR configurations. And the comparison of calculation results can be helpful in designing the optimal shape of TR in the preliminary design stage of gas generator. To this end, two different physical quantities also are selected as major measures of turbulent mixing in number description, such as perturbation energy and perturbation enstrophy. Perturbation energy represents the kinetic energy pumped into flow due to the agitation by TR and splash plate. Turbulent kinetic energy can also be transformed into flow vorticity as a source of flow mixing. And perturbation enstrophy is directly associated with flow mixing. [16] Perturbation energy is defined as the spatial integration of kinetic energy agitated by TR and perturbation enstrophy is the integral of vorticity perturbation over a given space. [17]

Perturbation energy; $\frac{1}{2V}\int_{\Omega}|\underset{\sim}{w}|^2\,dV$ (11)

Perturbation enstrophy; $\frac{1}{2V}\int_{\Omega}|\nabla\times\underset{\sim}{w}|^2\,dV$ (12)

Here, $\underset{\sim}{w}$ represents the perturbed velocity, V is a volume over the given space Ω.

$$\underset{\sim}{w} = \underset{\sim}{W} - \overline{\underset{\sim}{W}} \quad (13)$$

And W is an instantaneous velocity, $\overline{W}$ denotes an average velocity as defined in equation (14)

$$W = (u_x, u_y, u_z),\ \overline{W} = (\overline{u}_x, \overline{u}_y, \overline{u}_z) \quad (14)$$

As aforementioned, perturbation energy is a measure of the total energy input produced by TR, which can be transformed into vorticity for turbulent mixing. Meanwhile, perturbation enstrophy is the index to investigate the mixture degree occurring in the flow. Thus, the decrease in enstrophy along the axial direction shows the vorticity diminishes by dissipative mechanisms in the flow.

Figure 8 shows the distribution of perturbation energy and enstrophy for each case in the axial direction. Each curve on the graph was integrated over the sectional area of the chamber by the definition of perturbation energy and enstrophy. As expected, first three cases of 1, 2, and 3 show very similar behaviors of perturbation energy and enstrophy distribution even though the magnitude of perturbation energy and enstrophy over the whole chamber length differs somewhat from each other. The overall behavior of energy and enstrophy shows the monotonic decrease after a big jump at TR in case 1 to 3. Similar behavior of energy and enstrophy was found in the gas generator of case 4 calculated with TR having longer intrusion length. Calculation results suggest that the installation of TR can generate very similar turbulence distribution regardless of TR configuration but depending on the intrusion length.

However, the installation of splash plate may produce different behaviors of kinetic energy and enstrophy as shown in case 5. Perturbation energy is produced quite intensively showing a peak at TR and the formation of hill shaped energy is followed. And the perturbation energy drops very quickly within a short distance compared to other cases. Perturbation enstrophy increases abruptly at the location of TR and followed by the second increase behind splash plate. The gradual decrease approaches toward negligibly small value at 6 (correspond to the dimensional location of 200mm). This implies that vorticity diminishes and is so weak that turbulent mixing can not be actively dominant in the flow. Thus, the splash plate in case 5 may produce a quite large amount of turbulent kinetic energy at TR and around plate. And turbulent kinetic energy can be used for flow mixing enhancement in the region at TR and behind the plate. And the mixing completes in a short axial distance leaving no traces of turbulent energy in the downstream flow. This means flow in the downstream is homogeneously well mixed and no stratifications remain in the flow prior to turbine inlet.

Meanwhile, perturbation energy in case 1 to 3 and case 4 decreases monotonically up to the end of the chamber even perturbation enstrophy drops quickly in the middle of the chamber nearly the same location observed in case 5. This represents that turbulent agitation remains to the end of the chamber in case 1 to 4 even though turbulent mixing completes in the middle of the chamber. Thus, it can be summarized that the addition of splash plate is an effective way for mixing enhancement in that this will not leave any undesirable flow agitations prior to turbine inlet. The longer intrusion length of TR produces more power turbulent kinetic energy to the flow. However, the increased kinetic energy level can not be used in efficiently converted into mixing enhancement in the downstream because the formation of roll-up vortex at TR and the breakup are the only mechanism to produce turbulent mixing as observed in figure 7.

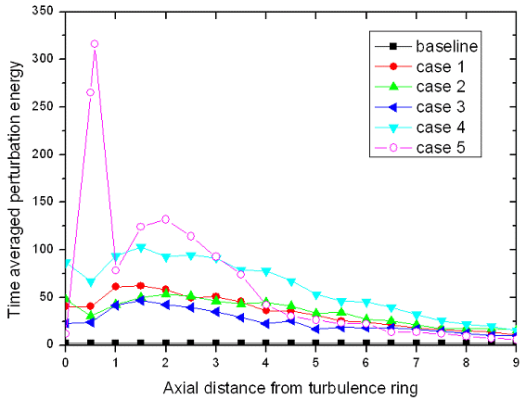

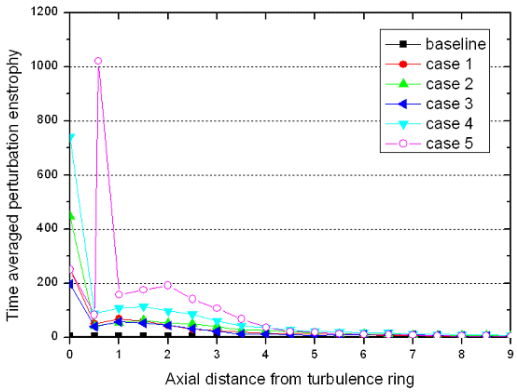

Fig 8. Perturbation energy and enstrophy distribution

Pressure drop is another physical measure in evaluating mixing performance in gas generator. The combustion in gas generator is assumed to take place in constant pressure condition. The installation of TR or splash plate and wall friction can induce pressure drops through viscous dissipation in the flow. Also, heat addition to the flow may cause pressure drops so called Rayleigh flow phenomenon. In the present study, viscous dissipation made by TR or splash plate is the primary concern in determining the mixing enhancement in isothermal flow. Figure 9 shows the pressure distributions of all cases along the center line in the axial direction. As seen in the figure, the behavior of pressure drop in all cases 1 to 4 occurred at TR and followed by the gradual recovery to the final value less than initial one. Also, pressure distributions in cases 1 to 4 have the similar behavior along the axial direction showing a gradual decrease across TR and followed by the recovery in the downstream to the chamber exit. And it is worth noting that the maximum pressure drops for all cases are within the range of 0.5% to 2.0% of initial pressure.

However, splash plate introduces pressure jump from TR to plate and showed similar behavior of pressure recovery after splash plate as observed in other cases. Pressure jump is related to the stagnation point on the plate located in the centerline. Final pressure drop in this case marks about 1% even though the maximum pressure drop is about 2% of initial pressure.

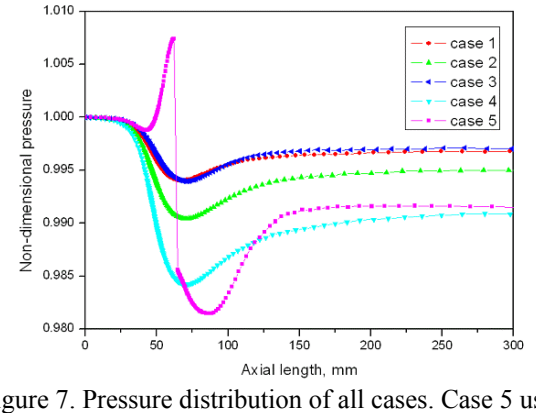

Figure 7. Pressure distribution of all cases. Case 5 used splash plate in the calculation

This behavior in splash plate case suggests that the adoption of splash plate with TR can take a better role of turbulent mixing in the downstream without causing too much pressure drop. It is worth noting that pressure recovery approaches toward a constant value if the axial location is over 200mm for all cases.

5. Summary and Conclusions

LES analysis was conducted by in-house CFD code to investigate the turbulence generation and interaction due to turbulence ring and splash plate in gas generator. Even though chemical reaction was not accounted for, the analysis can be useful in determining the turbulence characteristics generated by ring in the combustor. The calculation results show that the installation of turbulence ring can introduce additional turbulences and improve turbulent mixing in the downstream flow. However, the addition of splash plate in the downstream of TR produces better shape of perturbation energy and enstrophy distributions for turbulent mixing by forming the intensive vorticity behind plate. Also, pressure drop was found to be a reasonable level of about 1% of initial pressure compared to the pressure drops in other cases in the calculation. Even though the effect of location of splash plate on the turbulent mixing is not investigated yet, calculation results conclude the addition of splash plate can lead to the increase in perturbation energy and vorticity dramatically in the downstream of gas generator without causing too much pressure drops. Future study will be focused on the subject of optimal plate location to improve turbulent mixing with implantation of passive scalar technique.

References

1) Fureby, C., "Large Eddy Simulation of combustion instabilities in a jet engine afterburner model", 2000.
2) Weiss, J. M., Maruszewski, J. P., and Smith, W. A., "Implicit Solution of Preconditioned Navier-Stokes Equations Using Algebraic Multigrid", AIAA Journal, Vol. 37, No. 1, 1999, pp. 29-36.
3) Park, S. H., Lee, J. E., and Kwon, J. H., "Preconditioned HLLE Method for Flows at All Mach Numbers", AIAA Journal, Vol. 44, No. 11, 2006, pp. 2645-2653.
4) Choi, Y.-H., and Merkle, C. L., "The Application of Preconditioning in Viscous Flows," Journal of Computational Physics, Vol. 105, No. 2, 1993, pp. 207-223.
5) Venkateswaran, S., Li, D., and Merkle, C. L., "Influence of Stagnation Regions on Preconditioned Solutions at Low Speeds, "AIAA Paper 2003-0435, Jan. 2003.
6) Venkateswaran, S., and Merkel, C. L., "Dual Time Stepping and Preconditioning for Unsteady Computations," AIAA Paper 95-0078, Jan. 1995.
7) Buelow, P. E. O., Schwer, D. A., Feng, J., and Merkle, C. L., "A preconditioned Dual-Time,

Diagonalized ADI scheme for Unsteady Computations," AIAA Paper 97-2101, June 1997.
8) Pandya, S. A., Venkateswaran, S., and Pulliam, T. H., "Implementation of Preconditioned Dual-Time Procedures in OVERFLOW," AIAA Paper 2003-0072, Jan. 2003.
9) Jameson, A., "Time Dependent Calculations Using Multi grid with Applications to Unsteady Flows past Airfoils and Wings," AIAA Paper 91-1596, June, 1991.
10) Rigby, D. L., "Compact Spatial Differencing and Subiteration Time Marching in the PARC Code," AIAA Paper 96-0385, Jan. 1996.
11) Huzel, D. K., and Huang, D. H., "Modern Engineering for Design of Liquid Propellant Rocket Engine", Progress in Astronautics and Aeronautics, Vol. 147, AIAA, 1992, pp. 53-55, 155-218.
12) "Liquid Rocket Gas Generator", Space Vehicle Design Criteria, NASA SP 8081, 1974.
13) "Liquid Rocket Engine injectors", Space Vehicle Design Criteria, NASA SP 8089, 1974.
14) Lawver, B. R., "Test Verification of LOX/RP-1 High-Pressure Fuel/Oxidizer-Rich Preburner Designs," AIAA Paper #82-1153, Presented at the 18th Joint Propulsion Conference, Cleveland, OH. June 1982.
15) S. T. Kwon, C. Lee and J. W. Lee, "Development of Fuel Rich Gas Generator for $10ton_f$ Liquid Rocket Engine", AIAA 2004-3363, 40th Joint Propulsion Conference, July. 2004.
16) A. Balogh, and O. M. Aamo, Optimal Mixing Enhancement in 3D pipe Flow, IEEE Transaction on Control System Technology, pp. 27-41, Vol. 13, No. 1, 2005.
17) S. Kim, Design study of an Advanced Gas Generator, 29^{th} Joint Propulsion Conference, AIAA 93-2158